energies

MDPI

Review

Polyoxometalates as Electrocatalysts for Electrochemical Energy Conversion and Storage

Filipe M. B. Gusmão [1], Dušan Mladenović [2], Kristina Radinović [2], Diogo M. F. Santos [1] and Biljana Šljukić [1,*]

[1] Center of Physics and Engineering of Advanced Materials, Laboratory for Physics of Materials and Emerging Technologies, Chemical Engineering Department, Instituto Superior Técnico, Universidade de Lisboa, 1049-001 Lisbon, Portugal
[2] University of Belgrade, Faculty of Physical Chemistry, Studentski trg 12-16, 11158 Belgrade, Serbia
* Correspondence: biljana.paunkovic@tecnico.ulisboa.pt

Abstract: Polyoxometalates (POMs) are polyatomic ions with closed three-dimensional frameworks. Their unique structure contains a large number of redox active sites, making them promising electrocatalysts for electrochemical energy conversion and storage applications. Thus, this paper presents an overview of the use of POMs as electrocatalysts for electrochemical energy conversion and storage devices, such as batteries, supercapacitors, fuel cells, or water electrolyzers. A discussion of the viability of these materials as alternatives to noble metal-based electrocatalysts is made. The current status of these materials to respond to the challenges of converting modern energy systems into more sustainable ones is also envisaged.

Keywords: polyoxometalates; electrocatalysis; energy conversion and storage; hydrogen evolution reaction; oxygen evolution reaction; oxygen reduction reaction

Citation: Gusmão, F.M.B.; Mladenović, D.; Radinović, K.; Santos, D.M.F.; Šljukić, B. Polyoxometalates as Electrocatalysts for Electrochemical Energy Conversion and Storage. *Energies* **2022**, *15*, 9021. https://doi.org/10.3390/en15239021

Academic Editor: Adriano Sacco

Received: 22 October 2022
Accepted: 22 November 2022
Published: 29 November 2022

1. Introduction

Today's society faces one of its biggest challenges in the form of climate change. This makes the pursuit of energy storage and production options that do not emit greenhouse gases mandatory for all developed countries [1,2]. This endeavor takes several forms: the replacement of fossil-fueled vehicles with electrical ones, the production of electricity via renewable sources for all forms of electrical consumption, and finally, efficient energy storage. This last facet is a mandatory part of the equation when it comes to renewable energy production since it tends to fluctuate greatly during the day and throughout the year in terms of energy produced.

In the endeavor to solve these issues, a potentially viable option has been found. The concept of the "Hydrogen Economy", based on using hydrogen as an energy carrier, has now become a reality. However, most hydrogen comes from hydrocarbon reforming, a source of global pollution [3,4], which is certainly not sustainable. Using water electrolysis cells powered by renewable energy sources produces green hydrogen gas, a clean and efficient form of energy storage. Coupled with the fact that hydrogen can be fed to fuel cells to generate electricity, this makes the concept very interesting from a circular economy perspective [5].

Of course, this technology does not come without its limitations. Core reactions in water electrolyzers and fuel cells, oxygen evolution (OER) and oxygen reduction (ORR), as well as hydrogen evolution reaction (HER), have slow kinetics, requiring high overpotentials to obtain reasonable currents. Electrocatalysts are used to reduce the energy consumption in these reactions, with ruthenium oxide and platinum being the most efficient for OER and ORR/HER, respectively, but also high-cost materials. The ongoing search for low-cost, high-performance catalysts has proven to be difficult; most of these only operate in current ranges below 100 mA cm^{-2}, which is not satisfactory for production on an industrial scale.

Another problem in testing these materials is the difference between temperature, pressure, and electrolyte concentration values of small-scale lab cells compared with industry-scale ones, which will lead to significant divergence in electrolyte conductivity, ion migratory flux, and catalyst structural stability [6]. For this reason, the present review paper focuses on the use of polyoxometalates (POMs) to overcome the aforementioned problems. POMs have shown interesting properties for OER/ORR and HER electrocatalysis, with good activity and low cost. Furthermore, they were shown to lead to promising performance of different types of batteries and supercapacitors when employed as electrode materials.

POMs are polyatomic ions composed of three or more transition metal (e.g., Mo, V, W) oxyanions linked together by shared oxygen atoms to form closed three-dimensional frameworks, Figure 1. The unique structure of POMs, which leads to a large number of redox active sites, makes them promising for energy conversion and storage applications. The study of POMs has been very in-depth, and applications have been found in the fields of material sciences, medical applications, and catalysis, which this review will cover more closely. Concerning this last field, important properties have been observed in these materials, such as high thermal stability, high sensitivity to electricity, and resistance to oxidative decomposition, making them prime candidates for electrocatalytic study.

POMs demonstrate distinctive redox characteristics and the capability of reversibly uptaking as much as 24 electrons per cluster unit $[PMo_{12}O_{40}]^{3-}$ in the solid state [7–11]. This clearly indicates POMs as materials applicable for multi-electron transfer processes. The electrochemical behavior of POMs in terms of redox potential and number of electrons stored can be tailored additionally by, for example, the incorporation of redox-active metal centers through a chemical modification; such tailored-made POMs might be suitable for various electrochemical and electroanalytical applications [9].

POMs are normally insulators with only a few POMs demonstrating (semi-)conducting behavior. However, high electronic conductivity, often along with ionic conductivity, mainly protonic conductivity, is essential for the use of POMs as electrocatalysts in electrochemical energy conversion and storage devices. Thus, to use POMs in these devices, it is crucial to ensure adequate charge flow. Anchoring POMs through covalent or non-covalent means on nanostructured carbon materials, including carbon nanotubes (CNTs) and graphene, as conductive and high-surface area substrates, enables the mentioned charge flow [12]. "Wiring" of POMs to conductive organic polymers has also been suggested as a way to overcome the issue of their low conductivity [9].

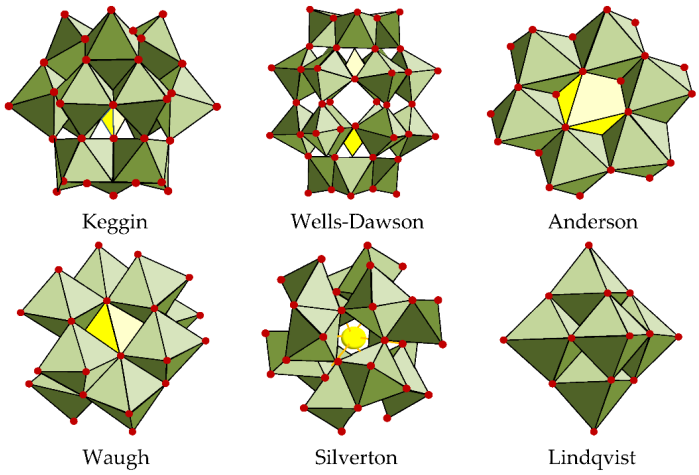

Figure 1. Polyoxometalates (POM) structures in polyhedral representations [13].

2. POMs as Electrocatalysts for the Oxygen Evolution Reaction (OER)

One of the reactions involved in water electrolysis is the oxygen evolution reaction (OER), in which water is oxidized to O_2. This reaction is further essential for the operation of metal-air batteries and unitized regenerative fuel cells. It has different mechanisms depending on the pH of the electrolyte solution, as shown in Figure 2. In any case, OER

encompasses all the problems that plague the production of hydrogen via electrolysis cells, as shown in Figure 3. It has high thermodynamic demands, and its kinetic obstacles lead to high activation energies. This translates into high overpotentials required for the reaction to start, making it evident that developing an efficient catalyst is mandatory when pursuing research in this field.

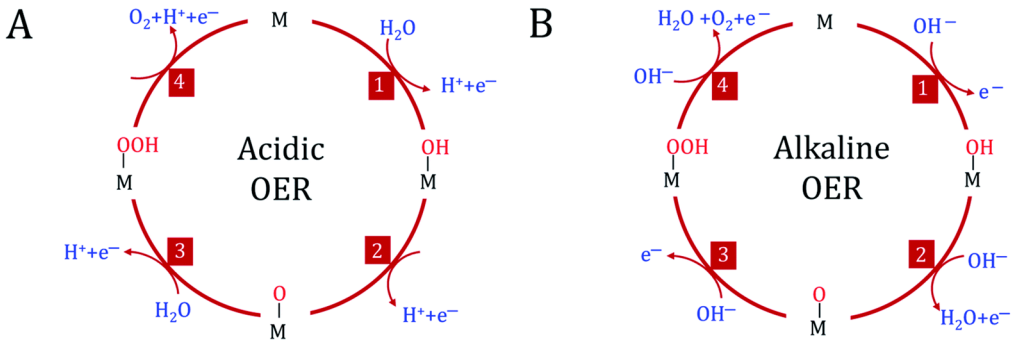

Figure 2. The schematic representation of the OER mechanism in acidic (**A**) and alkaline (**B**) media [14]. Each of the 4 steps corresponds to a single electron transfer.

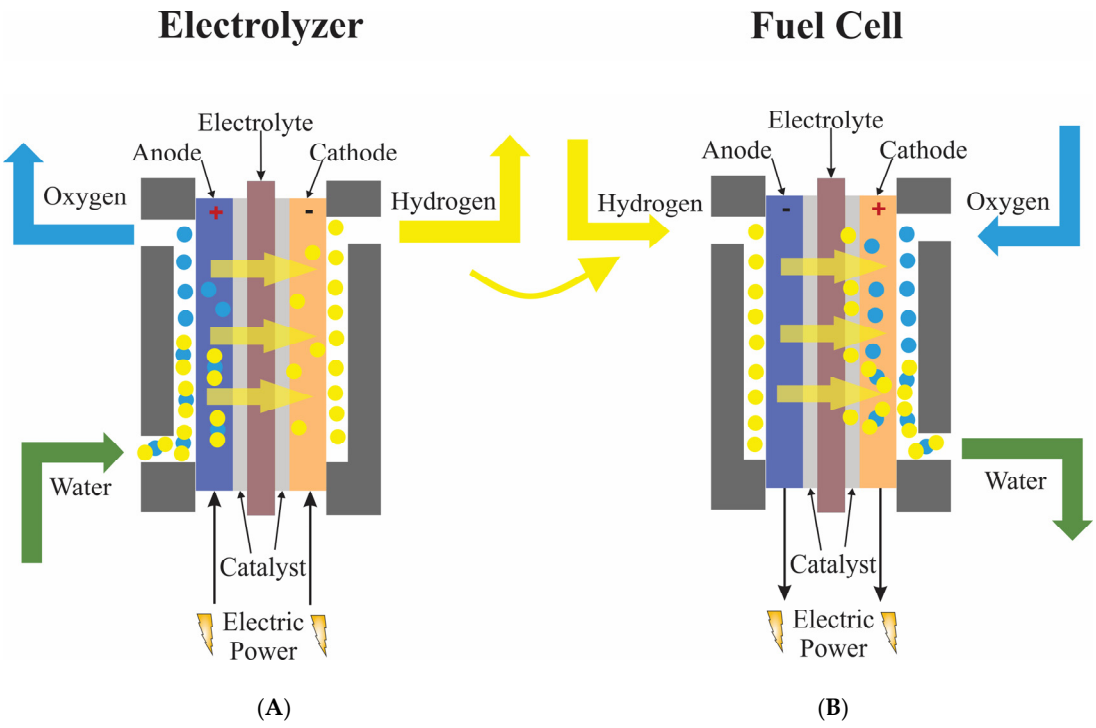

Figure 3. Schematic representation of a water electrolyzer (**A**) and a fuel cell (**B**).

Good performance when using POMs as catalysts for the OER has already been reported [15]. Removing metal oxygen entities creates empty spaces in the POM structure, creating so-called lacunary POMs. These are good inorganic ligands that stabilize multi-metal oxide clusters, creating a very robust structure that can be used to assemble catalytically active transitional metal-oxo clusters. So, different POMs can be studied for the desired catalytic effect, with various metals serving as the active sites.

2.1. Ruthenium POMs

One of the transition metals that can act as an active site of POMs is ruthenium (Ru). Even though Ru is a noble metal and, consequently, expensive, it should be mentioned that it has been demonstrated to be a powerful oxidant in a near-neutral pH. For example,

$[Ru_4O_4(OH)_2(H_2O)_4(SiW_{10}O_{36})_2]^{10-}$, or simply ($Ru_4Si_2$), has been reported as being highly active for OER [14,15], having a ratio of product formed per molecule of catalyst (turn-over number, TON) of up to 180 and initial d(TON)/dt (turn-over frequency, TOF) of up to 288 h^{-1} [16,17]. $[Ru_4(O)_5(OH)(H_2O)_4(PW_{10}O_{36})_2]^{9-}$, or ($Ru_4P_2$) was also shown to be able to catalyze the OER, but at a slightly lower efficiency [18].

Furthermore, studies involving Ru_4Si_2 combined with conductive materials have also been done. For example, anchoring the material to a conductive bed of multi-walled carbon nanotubes (MWCNTs) leads to higher electrocatalytic activity when compared to simply Ru_4Si_2-functionalized amorphous carbon [19]; this is most likely due to the enhanced electron transfer in MWCNTs. With these materials, a TOF of 300 h^{-1} was reached at an overpotential of 0.6 V [20].

Composite materials based on electrostatic immobilization of Ru_4Si_2 onto graphene followed by electrochemical deposition on glassy carbon have also been studied by Guo et al. [21]. This material showed good catalytic activity and stability under near neutral pH, with currents comparable to that of IrO_2 at an overpotential of 0.35 V.

According to Quintana et al. [22], another approach to increase the electrocatalytic performance of Ru_4Si_2 was to use graphene, covalently functionalized with organic, hydrogen-bonding, cations. This hybrid material shows an overpotential of 0.3 V to reach a current density of 0.150 mA cm^{-2}, and a negligible loss of performance even after 4 h of testing, all at neutral pH, performing at a higher efficiency than both isolated Ru_4Si_2 and its nanotube analogue.

2.2. Cobalt POMs

Cobalt (Co) is somewhat better than Ru in terms of higher abundance, but not particularly more sustainable. Namely, most of its reserves are located in countries with fewer regulations. which further leads to less emphasis on controlling the pollutants from the extraction of this metal [23]. Thus, Co may be considered a midway between the more sustainable transition metal-based POMs and the noble metal-based POMs.

Limani et al. [24] studied the viability of four cobalt phosphotungstate materials (MWCNT_N8_Co4, GF_N8_Co4, GF_ND8_Co4, and GF_NS8_Co4) as electrocatalysts. In alkaline media, with a pH of 13, all composites showed good performance, particularly GF_N8_Co4, which had an onset potential of 0.34 V vs. RHE and a maximum current of 70 mA cm^{-2} at 2 V vs. RHE, while also maintaining around 73–82% of its current after about 5.5 h. It is important to notice that these data mean that this electrocatalyst outperforms state-of-the-art IrO_2.

2.3. Manganese POMs

As mentioned, although Co is more abundant and consequently cheaper than Ru, its use comes with some drawbacks. So, better alternatives are yet to be found, for example, manganese (Mn). However, only a small number of Mn-POMs have been studied. The lack of Mn examples is not exclusive to POMs, because Mn oxide is generally much less active than the corresponding Co or Ni analogs when considering heterogeneous catalysis [25]. A good place to start the search for Mn-POMs that exhibit OER activity seems to be the Mn-analogue of the well-studied Co_4P_2, $Mn_4(H_2O)_2(PW_9O_{34})_2]^{10-}$, or simply ($Mn_4$) [26]. Even though electrochemical water oxidation experiments show initial activity comparable to the Co counterpart, the current density decreased very rapidly, becoming negligible in 30 min with the formation of an inactive MnO_x layer on the electrode.

Wu et al. [27] also studied another six POMs comprising different Mn-O clusters and Mn in different oxidation states: (Mn_2-POM), (Mn_4-POM), (Mn_6-POM-1), (Mn_6-POM-4), (Mn_{14}-POM), and (Mn_{19}-POM), both with these materials in solution, and then deposited on the surface of indium tin oxide (ITO) electrodes to form the composite films. It was found that Mn_{14}-POM displays the highest electrocatalytic performance toward oxygen evolution. It was also concluded that the oxidation state of Mn and the cubic structure

of Mn-O cluster are important factors impacting the POMs electrocatalytic performance for OER.

2.4. Nickel POMs

Extensive studies of Ni-based electrocatalysts for electrochemical energy-related applications showed that their performance often overcomes that of the benchmark electrocatalysts [28]. Nanostructured Ni-based materials have especially shown promising activity for oxygen electrode reactions, as well as HER.

When it comes to POMS, nickel POMs are some of the most recent ones; $[Ni_5(OH)_6(OH_2)_3(SiW_9O_{33})_2]^{12-}$ or (Ni_5Si_2) was only first reported in 2012 by Zhu et al. [29]. The research into this type of material continued with Singh et al. [30] who in 2018 reported a hybrid POM-supported Ni^{II} coordination complex, $[(Ni^{II}(bpy)_2(H_2O))(HCo^{II}W^{VI}{}_2O_{40})]_2{}^{3-}$, with Ni^{II} metal ion acting as the active center. This catalyst was highly stable and robust for OER at pH 7 having a high TOF of 18.49 (mol of O_2)(mol of Ni(II))$^{-1}$ s^{-1} and a Tafel slope of 168.41 mV dec^{-1}.

A simple one-step hydrothermal deposition of microcrystals of a Dexter–Silverton POM, $[Co_{6.8}Ni_{1.2}W_{12}O_{42}(OH)_4(H_2O)_8]$, on a commercial Ni foam, resulted in an industrially viable/applicable composite electrode for OER in alkaline electrolytes [31]. Namely, the overpotential to reach a current density of 10 mA cm^{-2} under OER polarization conditions was observed to be as low as 360 mV. The material's good activity towards OER was further reflected in the Tafel slope value of 126 mV dec^{-1}, accompanied by a faradaic efficiency of over 90%. Furthermore, the material demonstrated high mechanical and chemical stability and no detachment of the POM microcrystals from the metal foam support.

Similarly, $(C_5H_7N_2)_6[NiW_{12}O_{44}]$ showed an overpotential of 347 mV to reach 10 mA cm^{-2} complemented by long-term stability (up to 96 h) under OER polarization conditions in alkaline media [32]. NiO and WO_x (x = 1 or 2), with activity for OER, were generated in situ, further contributing to the electrocatalysis of OER.

Ni-POMs have also been shown to have a high photocatalytic activity to drive efficient water oxidation under visible light. Thus, $Na_{24}[Ni_{12}(OH)_9(CO_3)_3(PO_4)(SiW_9O_{34})_3]\cdot 56H_2O$, $Na_{25}[Ni_{13}(H_2O)_3(OH)_9(PO_4)_4(SiW_9O_{34})_3]\cdot 50H_2O$, and $Na_{50}[Ni_{25}(H_2O)_2OH)_{18}(CO_3)_2(PO_4)_6(SiW_9O_{34})_6]\cdot 85H_2O$ demonstrated high O_2 evolution TON of 128.2, 147.6, and 204.5, respectively [33]. The studied compounds' photocatalytic activity was attributed to the band gap structures, numerous active sites, and the favorable structural design of POMs.

2.5. Copper and Iron POMs

Yu et al. [34,35] studied two Cu-POMs clusters, where $[Cu_3(H_2O)_3(SbW_9O_{33})_2]^{12-}$ was shown to catalyze OER at neutral pH without decomposition under homogeneous electrochemical conditions. Interestingly, $[Cu_5(OH)_4(H_2O)_2(SiW_9O_{33})_2]^{10-}$, the POM that could photochemically catalyze the same reaction, showed negligible electrochemical activity under the same conditions.

Azmani et al. reported the activity of Fe-POMs in relation to Co-POMs in 2021 [36], comparing $[Fe^{III}{}_4(H_2O)_2(B\text{-}\alpha\text{-}PW_9O_{34})_2]^{6-}$ (Fe_4-WS) to its cobalt analog $[Co^{II}{}_4(H_2O)_2(B\text{-}\alpha\text{-}PW_9O_{34})_2]^{10-}$ (Co_4-WS). Still, it was found that Fe^{III} derivatives display lower OER activity than Co^{II}-POMs. These results are in agreement with the theoretical considerations, as the lower Tafel slope exhibited by Co_4-WS pointed to faster OER kinetics than in the case of Fe_4-WS. This owes to the lower activation barrier in the case of Co_4-WS. These activation barriers were determined using the computation of the transition state of one water molecule forming a hydrogen bond with a bridging oxygen [36].

Han et al. synthesized sub-nanometric heterometallic CoW and FeCoW clusters by a molecule-to-cluster approach starting from several different POMs (i.e., $[\{Co_4(OH)_3PO_4\}_4(SiW_9O_{34})_4]^{32-}$, $[\{Fe_2Co_2(OH)_3PO_4\}_4(SiW_9O_{34})_4]^{24-}$, and $[\{FeCo_3(OH)_3PO_4\}_4(SiW_9O_{34})_4]^{28-}$) as precursors [37]. The amount of Fe in the FeCoW clusters could be controlled by using POM precursors comprising a different number

of Fe atoms. Outstanding OER activity with overpotential to reach a current density of 10 mA cm^{-2}, η_{10}, as low as 192 mV, and a Tafel slope as low as 36 mV dec^{-1} was recorded for the most promising material.

A direct comparison of the performance of different transition metal-POM-based electrocatalysts is not simple/straightforward due to the different experimental conditions used in various studies reported in the literature, Table 1. For instance, theoretical considerations of various possible transition metal and heteroatom combinations for Weakley POMs led to the conclusion that the activity of metal sites for OER decreases in the order Ru > Mn~Co > Fe > Ni for this particular type of POMs [38]. Moreover, Cr Weakley POM with Al as the heteroatom is expected to show an overpotential as low as 310 mV, i.e., lower than that of a commercial IrO_2 electrocatalyst [38]. Still, when it comes to transition metal-based electrocatalysts, the use of a combination of Ni and Mo, Fe, or Co was demonstrated to lead to the highest number of active sites and thus the highest electrocatalytic performance for water electrolysis and other electrochemical energy conversion reactions [28].

Table 1. OER parameters of different POMs and their composites reported in the literature.

Catalyst	Electrolyte	η_{10} (mV)	Tafel Slope (mV dec^{-1})	Source
MWCNT_N8_Co4	0.1 M KOH	400	55	[24]
GF_N8_Co4	0.1 M KOH	340	67	[24]
GF_ND8_Co4	0.1 M KOH	490	68	[24]
GF_NS8_Co4	0.1 M KOH	460	62	[24]
Mono(aqua)nickel(II)	0.1 M phosphate buffer	-	168	[30]
$Co_{6.8}Ni_{1.2}W_{12}O_{42}(OH)_4(H_2O)_8$/Ni foam	0.1 M KOH	360	126	[32]
$(C_5H_7N_2)_6[NiW_{12}O_{44}]$	1 M KOH	347	-	[32]
Ru4POM	80 mM sodium phosphate	-	120	[39]
Co4POM	0.1 M KNO_3	-	80	[39]
NiP_4Mo_6	0.1 M KOH	-	73	[40]
Fe_2Ni_2@MWCNT_N6	0.1 M KOH	580	45	[41]
Fe_4@MWCNT_N6	0.1 M KOH	460	102	[41]
Ni_4@MWCNT_N6	0.1 M KOH	360	54	[41]
ZIF-8@ZIF-67@POM	1 M KOH	490	88	[42]
Ba[Fe_4-WS]/CP	50 mM potassium phosphate buffer with 1 M KNO_3	-	99	[36]
Ba[Co_4-WS]/CP	50 mM potassium phosphate buffer with 1 M KNO_3	-	73	[36]
PBA@POM	1 M KOH	440	235	[43]
1-CoW	1 M KOH	240	53	[37]
2-CoFeW	1 M KOH	224	43	[37]
3-CoFeW	1 M KOH	205	38	[37]

Co_4—$[Co_4(H_2O)_2(PW_9O_{34})_2]$; Mono(aqua)nickel(II)—$[Ni^{II}(2,2-bpy)_3]_3[Ni^{II}(2,2-bpy)_2(H_2O)HCo^{II}W^{VI}_{12}O_{40}]_2{\cdot}H_2O$; Ru_4POM—$[Ru_4O_4(OH)_2(H_2O)_4(\gamma-SiW_{10}O_{36})_2]^{10-}$; Co_4POM—$[Co_4(H_2O)_2(PW_9O_{34})_2]^{10-}$; NiP_4Mo_6—$Ni_3[Mo_6O_{12}(OH)_3(HPO_4)_3(PO_4)]_2{\cdot}4bpe{\cdot}10H_2O$, bpe = 4,4-vinylene-dipyridine; Fe_2Ni_2—$Na_{14}[(FeOH_2)_2Ni_2(As_2W_{15}O_{56})_2]{\cdot}55H_2O$; Fe_4—$(Na_{12}[(FeOH_2)_2Fe_2(As_2W_{15}O_{56})_2]{\cdot}54H_2O$; Ni_4—$Na_{12}[(NiOH_2)_2Ni_2(As_2W_{15}O_{56})_2]{\cdot}54H_2O$; ZIF-8@ZIF-67@POM—zeolitic imidazolate frameworks@$H_3[PW_{12}O_{40}]{\cdot}nH_2O$; Ba[$Fe_4$-WS]—$[Fe^{III}_4(H_2O)_2(B\text{-}\alpha\text{-}PW_9O_{34})_2]^{6-}$ and Ba[Co_4-WS]/CP—$[Co^{II}_4(H_2O)_2(B\text{-}\alpha\text{-}PW_9O_{34})_2]^{10-}$, both with carbon paste (CP); POM in PBA@POM—$H_3PMo_{12}O_{40}$.

3. POMs as Electrocatalysts for the Hydrogen Evolution Reaction (HER)

Although the OER is deliberated as an efficiency-limiting process in electrolytic water splitting, the hydrogen evolution reaction (HER), which involves several steps (Figure 4), also poses several challenges that must be tackled. As stated before, hydrogen production is a possible solution to the world's current energy problems, but existing platinum-based electrocatalysis solutions need to be replaced by lower-cost alternatives. POMs are potential candidates as electrocatalysts for green hydrogen production. They have been shown to have a close enough performance to commercial carbon-supported platinum (Pt/C), the most used electrocatalyst for acidic and alkaline media, while being considerably cheaper.

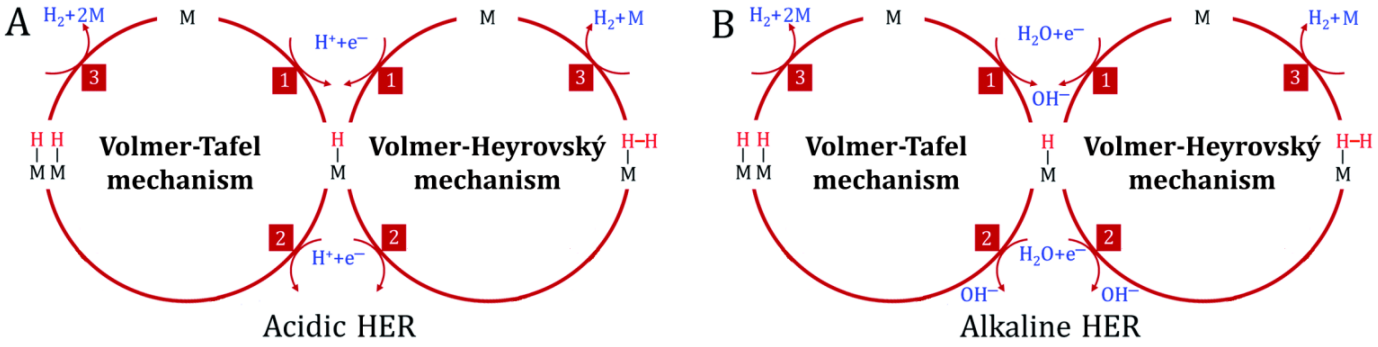

Figure 4. The schematic representation of the HER mechanisms in acidic (**A**) and alkaline (**B**) conditions, showing the 3 steps involved in each mechanism.

Singh et al. [44] studied the copper-based POM [{Cu^{II}(2,2′-bpy)(H2O)$_2$}] [{$Co^{II}W^{VI}_{12}O_{40}$}{Cu^{II}(2,2′-bpy)(H2O)}{Cu^{II}(2,2′-bpy)}]·2H_2O, close to neutral pH. In this, POM {Cu^{II}(2,2′- bpy)(H2O)$_2$}$^{2+}$ acts as the active center, catalyzing the HER. The overpotential to reach 1 mA cm^{-2} was determined to be 520 mV and TOF to be 6329 mol of H_2 evolved per mole of Cu atom per hour at the current density of 1 mA cm^{-2}. This was a huge increase when compared with previously reported Cu clusters, whose TOF was 457 mol of H_2 per mol of catalyst per hour at 817 mV [45]. These values are also more favorable than those of other complexes reported in the literature; namely, Ni- [46] and Co-complexes [47] were found to have TOF values of only 970.45 and 871.17 mol of H_2 mol catalyst^{-1} h^{-1}, respectively, both measured at an overpotential of 837 mV.

Several Dexter–Silverton POM/Ni foam composites (NiM-POM/Ni; M=Co, Zn, Mn) were shown to be efficient electrocatalysts for HER in alkaline media (1 M KOH). NiCo-POM/Ni exhibited the highest activity towards HER in terms of the lowest overpotential (64 mV) to reach 10 mA cm^{-2} accompanied by a low Tafel slope of 75 mV dec^{-1} and faradaic efficiency as high as ca. 97%. Moreover, NiCo-POM/Ni was observed to be both mechanically and chemically stable [48].

Ni-based polyoxovanadate $K_2[Ni(H_2O)_6]_2[V_{10}O_{28}]\cdot 4H_2O$ was found to exhibit homogeneous electrocatalytic activity for HER in acidic media with a low overpotential of 127 mV to reach half of the maximum current and TOF of 2.1 s^{-1} at pH 2.3 [49]. It is worth noting that $[Ni(H_2O)_6]^{2+}$ on its own does not exhibit any activity for HER, only when present in a POM matrix. Additionally, high stability, i.e., no decomposition, of $K_2[Ni(H_2O)_6]_2[V_{10}O_{28}]\cdot 4H_2O$ under HER polarization conditions was detected.

In 2020, Wang et al. [50] prepared and investigated the electrocatalytic properties of another three copper-based POMs, {Cu_2(3-bptzp)$_3$(H_2O)$_4$[$SiW_{12}O_{40}$]}·H_2O, {Cu_2(3-bptzpe)$_2$(H_2O)$_8$[$SiW_{12}O_{40}$]}·4H_2O, and {Cu_2(3-bptzh)$_3$(H_2O)$_6$[$SiW_{12}O_{40}$]}, where (3-bptzp = 1,4-bis (5-(3-pyridyl)- tetrazolyl)- butane; 3-bptzpe = 1,4-bis(5-(3-pyridyl)tetrazolyl)-pentane, and 3-bptzh = 1,4-bis(5-(3-pyridyl)tetrazolyl)-hexane). All these POM-based metal-organic complexes exhibited good electrocatalytic activity under alkaline and acidic media. In particular, {Cu_2(3-bptzp)$_3$(H_2O)$_4$[$SiW_{12}O_{40}$]}·H_2O achieved a current density of 10 mA cm^{-2} at an overpotential of 59.4 mV vs. RHE, leading to a Tafel slope of 74.2 mV dec^{-1} in a 0.1 M KOH solution. It was further determined that even though

the materials were stable under the full pH range, acidic media led to higher overpotentials and Tafel slopes.

Fernandes et al. [51] studied three further nanocomposites based on POMs on reduced graphene oxide (rGO) for HER in acidic media, and they were all shown to have overpotentials to reach 10 mA cm^{-2}—very close to the state-of-the-art commercial Pt/C. P2W18@rGF_ox, P5W30@rGF_ox, and P8W48@rGF_ox were prepared by an easy and cost-effective one-step electroreduction of POM@rGF_ox. P5W30@rGF_ox showed the best activity with a Tafel slope of 33 mV dec^{-1}, but even the worst one, P8W48@rGF_ox, had a Tafel slope as low as 41 mV dec^{-1}, both relatively close to that of commercial Pt/C, 30 mV dec^{-1}.

A dual-atom catalyst comprising O-bridged W-Mo atoms onto N-doped graphene vacancies (with W-O-Mo-O-C configuration) was developed by controlled self-assembly of POMs and subsequent nitridation [52]. The performance of the prepared W-Mo heterodimer electrocatalyst overpasses the performance of homodimer Mo-Mo and W-W and it is comparable to that of Pt/C, along with remarkable stability under HER polarization conditions in a wide pH range.

Novel heterostructure comprising zinc iron oxide ($ZnFe_2O_4$) and POM nanoplates (POM–$ZnFe_2O_4$) synthesized via a hydrothermal method exhibited excellent performance for both HER and OER [53]. Thus, the current densities of 20 and 50 mA cm^{-2} were reached at low overpotentials of 268 and 356 mV, respectively, under HER polarization conditions, and at 220 and 290 mV, respectively, under OER polarization conditions. Moreover, an electrolytic cell with POM–$ZnFe_2O_4$ serving both as the cathode and as anode delivered a current density of 10 mA cm^{-2} at an operating voltage of 1.53 V. The electrochemical activity of POM–$ZnFe_2O_4$ overpassed that of commercial Pt/C and RuO_2 catalysts for HER and OER, respectively, and some catalysts recently reported in the literature. The acceleration of HER and OER by POM–$ZnFe_2O_4$ most likely originates in the modulation of its electronic and chemical characteristics along with the creation of heterojunction of $ZnFe_2O_4$ and POM, as well as its high electrochemically active surface area (ECSA).

All these studies on POMs for HER show excellent potential for this class of compounds. They also encourage further work with other materials to be combined with the POMs, creating highly conductive nanocomposites. These mainly include nanostructured carbon materials, such as the already mentioned graphene and reduced graphene oxide, carbon nanotubes, as well as conductive polymers.

4. POMs as Electrocatalysts for the Oxygen Reduction Reaction (ORR)

The presence of transition metal ions in the POM framework enables fine-tuning of their redox potentials. Incorporating a POM-based catalyst can increase the rate of the electroreduction process and lower the overpotential. The POM is said to "act as a powerful electron reservoir" and can usually provide electrons to other species [53].

The oxygen reduction reaction (ORR) is an integral process in fuel cells and metal-air batteries. Its catalysis is crucial because it presents sluggish kinetics, requiring high overpotentials to start. Generally, catalysts for ORR applications are selected to preferentially have a four-electron transfer mechanism, where O_2 is reduced to water (Equations (1) and (4) for alkaline and acidic media, respectively), in detriment to the two-electron pathway, which produces hydrogen peroxide (H_2O_2) (Equations (2), (3), (5), and (6) for alkaline and acidic media, respectively) [54]. Still, according to Zheng et al. [40], the two-electron transfer pathway can sometimes be desirable, as it is a safer and cheaper way to produce H_2O_2 than current technology, and POMs could also serve to catalyze this process.

Alkaline electrolyte

(a) Direct 4-electron pathway

$$O_2 + 2H_2O + 4e^- \rightarrow 4OH^- \ E^\circ = 0.401 \text{ V} \quad (1)$$

(b) Peroxide (2-electron) pathway

$$O_2 + H_2O + 2e^- \rightarrow HO_2^- + OH^- \ E^\circ = +0.065 \text{ V} \quad (2)$$

$$HO_2^- + H_2O + 2e^- \rightarrow 3OH^- \ E^\circ = +0.867 \text{ V} \quad (3)$$

Acidic electrolyte

(a) Direct 4-electron pathway

$$O_2 + 4H^+ + 4e^- \rightarrow 2H_2O \ E^\circ = +1.229 \text{ V} \quad (4)$$

(b) Peroxide (2-electron) pathway

$$O_2 + 2H^+ + 2e^- \rightarrow H_2O_2 \ E^\circ = +0.67 \text{ V} \quad (5)$$

$$H_2O_2 + 2H^+ + 2e^- \rightarrow 2H_2O \ E^\circ = +1.77 \text{ V} \quad (6)$$

Another critical factor for the optimal running of rechargeable metal-air batteries or unitized regenerative fuel cells is bifunctionality—the ideal electrocatalysts should be active for both OER and ORR. For fuel cell applications, it is also important to find catalysts selective for ORR, i.e., "resistant" to fuel (for instance, methanol) crossover.

Zhang et al. [55] reported the efficiency of various POM-based materials for ORR, involving different supports for Ni and Co POM core. The supports were thermalized triazine-based frameworks (TTFs), fluorine-doped TTF (TTF-F), and rGO. All compared favorably to commercial Pt/C, and particularly $\{(PW_9)_2Ni_7\}/\{Cu(ethylenediamine)_2\}$/TTF-F as the first example of POM-based noble metal-free ORR catalyst that possessed comparable ORR activity to Pt/C while having much better stability in neutral medium. At this pH, Cu_6Ni_7/TTF-F, Cu_6Ni_7/rGO, and Cu_6Ni_7/C were the first examples of POM-based electrocatalysts that could support the one-step reduction of oxygen to water.

Liu et al. recently reported a novel top-down POM-based single-atom catalyst design approach. Immobilization of POM-single site catalysts on high surface-area mesoporous carbon at high loading was demonstrated [56]. Keggin-polyoxomolybdate $[PMo_{12}O_{40}]^{3-}$ was used as a precursor for anchoring POM-like molybdenum (VI)-oxo subnanometer clusters ($[Mo\text{-}oxo]_n$, n = 1–20) onto carbon material. Such prepared material exhibited outstanding electrocatalytic activity for ORR, comparable to or even superior to that of commercial Pt/C catalysts.

Marques et al. [41] recently characterized three Fe and Ni-based POMs on MWCNTs, $(Na_{12}[(FeOH_2)_2Fe_2(As_2W_{15}O_{56})_2]\cdot 54H_2O$, $Na_{12}[(NiOH_2)_2Ni_2(As_2W_{15}O_{56})_2]\cdot 54H_2O$, and $Na_{14}[(FeOH_2)_2Ni_2(As_2W_{15}O_{56})_2]\cdot 55H_2O)$, in alkaline media. They all showed good ORR performances, having onset potentials of ca. 0.80 V vs. RHE and diffusion-limited current densities between −3.19 and −3.66 mA cm^{-2}. Stability tests showed Fe_4@MWCNT_N6 and Fe_2Ni_2@MWCNT_N6 to be the most promising, maintaining 84 and 80% of the current, respectively, after 12 h. Lastly, it was concluded that the number of electrons transferred per molecule of O_2 was close to three, suggesting a mixed 2e–4e mechanism.

RuPOM demonstrated high bifunctional activity for OER/ORR when combined with Ketjenblack (KB) carbon [57]. Its activity for OER was superior to that of commercial Pt/C catalysts and somewhat inferior in the case of ORR. Nevertheless, when it comes to the specific activity, i.e., the current density per mass of a precious metal, RuPOM significantly overpasses Pt/C. Thus, RuPOM/KB (in 8:2 ratio) gave 25- and 11-times higher ORR specific current density than RuO_2/KB and Pt/C, respectively. A seawater battery employing RuPOM/KB as a bifunctional catalyst for both OER and ORR exhibited notably

improved performance, as evidenced by a decreased potential difference between charging (OER) and discharging (ORR) from 1.30 to 0.76 V, and an increase of the output power.

Limani et al. [24] reported good ORR performance of MWCNT_N8_Co4, GF_N8_Co4, GF_ND8_Co4, and GF_NS8_Co4. These composites presented onset potentials in the range 0.83–0.85 V vs. RHE and a number of exchanged electrons of ca. 4, indicating that ORR proceeds as a direct four-electron reduction of oxygen to water. Moreover, these composites exhibited good tolerance to methanol crossover with ORR current retention of 88–90% and good stability with current retention of 73–82% after 20,000 s at 0.55 V vs. RHE. Table 2 summarizes ORR data reported in the literature for different POMs and POM-based materials.

Table 2. ORR parameters of different POMs and their composites reported in the literature.

Catalyst	Electrolyte	E_{onset} (V vs. RHE)	Tafel slope (mV dec^{-1})	Source
MWCNT_N8_Co4	0.1 M KOH	0.85	41	[24]
GF_N8_Co4	0.1 M KOH	0.83	50	[24]
GF_ND8_Co4	0.1 M KOH	0.85	90	[24]
GF_NS8_Co4	0.1 M KOH	0.84	40	[24]
NiP_4Mo_6	0.1 M KOH	-	106	[40]
S-NiP_4Mo_6	0.1 M KOH	-	98	[40]
Fe_4@MWCNT_N6	0.1 M KOH	0.80	35	[41]
Ni_4@MWCNT_N6	0.1 M KOH	0.80	35	[41]
Fe_2Ni_2@MWCNT_N6	0.1 M KOH	0.81	38	[41]
Pd_8Ni_2/rGO-POM	0.1 M KOH	0.90	60	[58]
$Co_4(PW_9)_2$@SWCNT	0.1 M KOH	0.77	68	[59]
$Co_4(PW_9)_2$@GF	0.1 M KOH	0.89	71	[59]
$Co_4(PW_9)_2$@N-CNT	0.1 M KOH	0.90	92	[59]
$Co_4(PW_9)_2$@N-FLG	0.1 M KOH	0.89	63	[59]
$Co_4(PW_9)_2$@Pt/C	0.1 M KOH	-	89	[59]
Mo-based species #1	0.1 M KOH	0.75	109	[56]
Mo-based species #2	0.1 M KOH	0.88	68	[56]
Mo-based species #3	0.1 M KOH	0.93	44	[56]

Co_4—$[Co_4(H_2O)_2(PW_9O_{34})_2]$; NiP_4Mo_6—$Ni_3[Mo_6O_{12}(OH)_3(HPO_4)_3(PO_4)]_2 \cdot 4bpe \cdot 10H_2O$, bpe = 4,4-vinylene-dipyridine; Fe_2Ni_2—$Na_{14}[(FeOH_2)_2Ni_{i2}(As_2W_{15}O_{56})_2] \cdot 55H_2O$; Fe_4—$(Na_{12}[(FeOH_2)_2Fe_2(As_2W_{15}O_{56})_2] \cdot 54H_2O$; Ni_4—$Na_{12}[(NiOH_2)_2Ni_2(As_2W_{15}O_{56})_2] \cdot 54H_2O$; Pd_8Ni_2—$H_3[PMo_4W_8O_{40}]$; $Co_4(PW_9)_2$@X—$[(Co_4(PW_9)_2)_7H_3[Co_4(H_2O)_2(PW_9O_{34})_2]$, X—single-walled carbon nanotubes (SWCNT), graphene flakes (GF), carbon nanotubes doped with nitrogen (N-CNT), or nitrogen-doped few layer graphene (N-FLG).

5. POMs for Batteries and Supercapacitors

A particularly difficult challenge for energy storage today is the development of rechargeable, high-performance, low-cost, and environmentally friendly batteries. Namely, new electrode materials that can lead to higher voltages and higher capacities need to be developed, and POMs have contributed to this development.

5.1. Lithium-Ion Batteries

Lithium-ion batteries (LIBs) (Figure 5) represent the currently most used energy storage devices due to their high voltage (>3.5 V), high energy density (<200 W h kg^{-1}), and reasonably long cycle life. Typically, lithium transition metal oxides including $LiCoO_2$, $LiMn_2O_4$, and $LiFePO_4$, are employed as cathodes in LIBs. Still, these materials suffer from a decrease of capacity during cycling as well as scarcity and high price, specifically

cobalt-based ones. Graphite is the most frequently employed anode in commercial LIBs. Still, graphite's low capacity limits its viability in large-scale systems. Bearing in mind the limitations of current cathode and anode materials used in LIBs, great attention has been devoted to the development of novel materials for this type of battery. POMs have been studied for use in the field of LIBs with their electrochemical performance being enhanced by the usage of nanosized particles and/or mixing them with highly electrically conductive materials. Additionally, POMs molecular clusters show multielectron redox properties as individual molecules, making their cycling stability and capacity independent of their crystalline stability. For instance, using polyoxomolybdate $(NH_4)_6[NiMo_9O_{32}]$ nanoparticles with KB carbon as cathode material led to an initial capacity discharge of 490 mA h g^{-1} with a capacity retention as high as 87.6% after 50 cycles at 17 mA g^{-1} [60]. Employing Mn-Anderson-type POM on single-walled carbon nanotubes as the anode material led to an initial capacity discharge as high as 3405.4 mA h g^{-1}, although with low-capacity retention (ca 27.4% after 100 cycles at 0.5 mA cm^{-2}) [61].

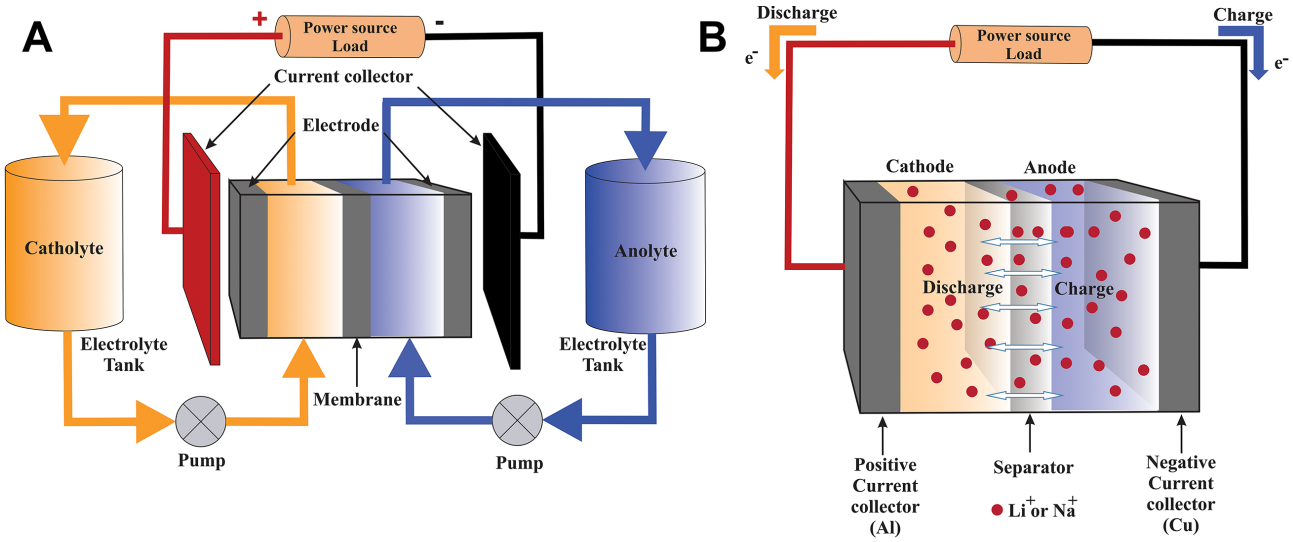

Redox flow battery schematic

Li-ion or Na-ion battery schematic

Figure 5. Schematic representation of a redox flow battery (adapted from [62]) (**A**) and a metal (Li, Na)-ion battery (**B**).

5.2. Sodium-Ion Batteries

Sodium-ion batteries (SIBs) are a promising alternative to LIBs for large-scale energy storage applications, bringing the advantage of a high abundance of sodium and thus lower cost. The possibility of employing aluminum as a low-cost current collector for both anode and cathode further lowers the price of this type of battery compared to LIBs. The use of aluminum is possible since sodium and aluminum do not form an alloy, unlike lithium and aluminum. However, this low cost comes with a problem: SIBs energy density is lower than LIBs as a consequence of the large radius of the Na^+ ions, large atomic weight compared to lithium, and low operating potential [63]. A possibility to overcome such problems is the use of new cathode materials. Therefore, this area of study has garnered tremendous attention lately. Liu et al. [64] and Chen et al. [65] studied POM-based materials for cathodes, while Hartung et al. [66] and Lin et al. [67] focused on anode materials.

$Na_2H_8[MnV_{13}O_{38}]$ (NMV) [64] as SIB cathode demonstrated a high specific capacity of 190 mA h g^{-1} (at 0.1 C) with high retention of, for instance, 81% at 0.2 C. The material's high performance was attributed to its "electron/Na^+-ion sponge" behavior with its structure providing numerous diffusion channels for Na^+ ions. The main contributor to its high capacity is the acceptance of 11 electrons/Na^+ per mole. The good rate capability is enabled by the material's flexible 2D lamellar network with 1D open channels providing numerous migration pathways for Na^+ ions. Finally, the good cycling stability is due to the formation

of $[MnV_{13}O_{38}]_{20}$ with size expansion upon insertion of Na^+ ions of ca. 7.5% compared to the parental $[MnV_{13}O_{38}]_9^-$.

Nanosized polyoxovanadate $Li_7V_{15}O_{36}(CO_3)$ [65] envisaged to enable the transport of large cations, including Na^+, demonstrated a high specific capacity of 240 mA h g^{-1} (at 50 mA g^{-1}) and led to a specific energy of 390 W h kg^{-1} when employed as the cathode of a rechargeable SIB.

$Na_6[V_{10}O_{28}].16H_2O$ [68] and $Na_7[H_2PV_{14}O_{42}]$ [67] as the SIB anode attained a capacity of ca. 276 (at 20 mA g^{-1}) and 322 mA h g^{-1} (at 25 mA g^{-1}), respectively, along with good cycling stability in case of both studied materials. For instance, capacity retention in the case of $Na_7[H_2PV_{14}O_{42}]$ was as high as 87% upon 120 cycles.

Still, it was generally concluded that storage capacities in SIBs were much lower than in LIBs, as shown in Table 3. This could be explained by low kinetics resulting from a Na_2O passivating film layer formed during the first charge/discharge cycles.

Table 3. Performance of different types of batteries involving POMs and their composites reported in the literature.

Material	Batteries	Electrode	Initial Discharge Capacity (mA h g^{-1})	Current/Current Density/Rate	Capacity Retention (%)	Cycle Number	Source
ANM/KB	LIBs	cathode	490	17 mA g^{-1}	87.6	50	[60]
Mn-Anderson/ SWNT	LIBs	anode	3405.4	0.5 mA cm^{-2}	27.4	100	[61]
Ni-POM	LIBs	anode	1325	100 mA g^{-1}	54	50	[69]
HP-NENU-5/CC	LIBs	anode	~2346	200 mA g^{-1}	73	100	[70]
HP-HKUST-1/CC	LIBs	anode	1259	200 mA g^{-1}	74.5	100	[70]
HP-PMo_{12}/CC	LIBs	anode	1147	200 mA g^{-1}	88	100	[70]
POMOFs-based $Pmo_{10}V_2$/rGO	LIBs	anode	2367.8	50 mA g^{-1}	45	100	[71]
PMO12/PANI/MWNTs	LIBs	anode	1572	0.5 mA cm^{-2}	63.6	100	[72]
Composite 1/SWNTs	LIBs	anode	1469	100 mA g^{-1}	67.3	100	[73]
$Li_7[V_{15}O_{36}(CO_3)]$	LIBs	cathode	170	2 A g^{-1}	84	100	[74]
Pmo_{12}	SIBs	anode	15.5	1.0 A g^{-1}	5.2	100	[75]
Pmo_{12}/MIL-88B/GO	SIBs	anode	430.2	1.0 A g^{-1}	67	100	[75]
Pmo_{12}/MIL-53/GO	SIBs	anode	152.4	1.0 A g^{-1}	40	100	[75]
Pmo_{12}/MIL-101/GO	SIBs	anode	44.5	1.0 A g^{-1}	18.6	100	[75]
Pmo_{12}/GO	SIBs	anode	103.4	1.0 A g^{-1}	-	100	[75]
$Li_7V_{15}O_{36}(CO_3)$	SIBs	cathode	171	0.1 A g^{-1}	85	100	[65]
$Na_6[V_{10}O_{28}]$	SIBs	anode	300	20 mA g^{-1}	96	10	[66]
$Na_7[H_2PV_{14}O_{42}]$	SIBs	anode	397	25 mA g^{-1}	71	120	[67]
$Li_5BW_{12}O_{40}$-Lil	RFBs	-	24.8	100 mA g^{-1}	86.6	100	[76]
rGO-POMs HENFs	RFBs	-	-	4.0 A g^{-1}	97	250	[77]
all-$H_6[CoW_{12}O_{40}]$	RFBs	-	13.6	25 mA cm^{-2}	99	30	[78]

5.3. Redox Flow Batteries

Redox flow batteries (RFBs) might be considered ideal for stationary applications. This type of battery uses two electrolytes containing different electroactive species, stored outside the cell and continually pumped in, as shown in Figure 5 [68]. Two electrolyte solutions are separated by a membrane preventing their direct mixing but allowing the passage of ions. Such a unique construction design and operational mechanisms allow a RFB to be sized to meet the requirements of various energy and power demands [79].

POMs have been studied in RFBs as a strategy for enhancing their electrochemical performance [62,80,81]. Pratt et al. [82] developed three phosphorus-based POMs

(A-a-$PV_3W_9O_{40}^{6-}$, B-a-$PV_3W_9O_{40}^{6-}$, and $P_2V_3W_{15}O_{62}^{9-}$) for use as the electroactive components of RFBs electrolytes. The electrochemical measurements showed good pairs to act as positive and negative electroactive species, such as ($P^{VI}V_3W^{VI}{}_9O_{40}^{9-}/P^{V}V_3W^{VI}{}_9O_{40}^{6-}$) and ($P^{VI}V_3W^{VI}{}_9O_{40}^{9-}/P^{VI}V_3W^{V}{}_3W^{VI}{}_6O_{40}^{12-}$). However, the studied POMs still present low coulombic efficiency and poor cycling stability, a challenge that needs to be overcome if POMs are to be used in RFBs.

As seen in many other applications, the hybridization of POMs with other materials has been proposed to increase their electrochemical activity. Dubal et al. [77] proposed the hybridization of graphene and POMs to generate electroactive nanofluids for application in rGO/phosphomolybdate-based RFBs. These devices showed encouraging electrochemical features, including a specific capacitance of 305 F g^{-1} as well as durable coulombic efficiency (~77–79%) after 2000 cycles. Even though these results still pale in comparison to their vanadium counterparts, more effort and new approaches may lead to breakthroughs in using POMs in electroactive nanofluids of RFBs.

5.4. Supercapacitors

Supercapacitors (SCs) are praised for their high energy storage capacity and ability to deliver it at a higher power output compared to batteries. Their other advantages include durable cycle life, long-term stability, the capability of delivering a high current, and remarkable energy efficiency. Thus, SCs are perfect for applications requiring a primarily large number of quick charge/discharge cycles instead of long-lasting compact energy storage; for instance, they are used for burst-mode power delivery in different types of vehicles, elevators, and forklifts. Still, they suffer from a rather low cell voltage and their energy density could be further increased. POMs have been suggested as electrode materials suitable for pseudo-capacitors. Namely, supercapacitors can be classified in three groups: electric double layer (EDL) capacitors, pseudo-capacitors, and hybrid capacitors, having different charge storage mechanisms, as shown in Figure 6.

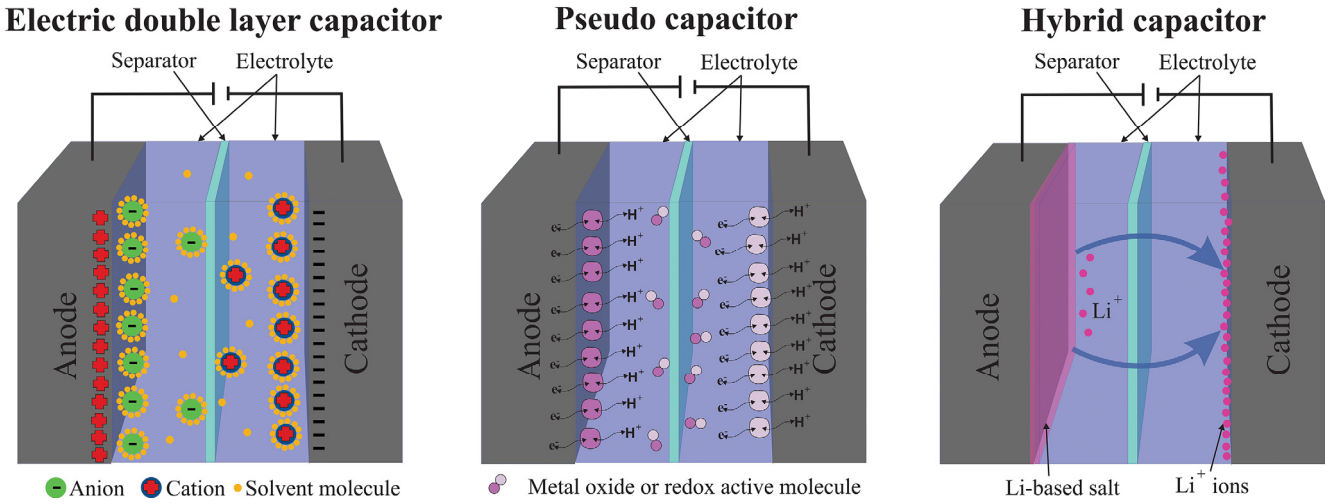

Figure 6. Schematic representation of the different types of supercapacitors.

Electric double-layer capacitors store charge by the reversible electrostatic accumulation of ions at the electrode/electrolyte boundary. Typically, high-surface area, porous carbon materials are employed in this category of SCs with graphene being considered the benchmark material [83]. The search for the optimal materials for EDL capacitors has led to achieving EDL capacitances in the 200–300 F g^{-1} range. [84] Extrinsic pseudocapacitive behavior is another favorable approach for increasing energy density. In this case, electroactive species react with surface functional moieties in a rapid reversible redox reaction [85]. Electrode materials used in pseudocapacitors include transition metal (such as Mn or Ru) oxides, heteroatom-doped carbon materials, and conducting polymers. POMs, with a high

surface-to-bulk ratio and metal species with a number of different redox states, seem to be great contenders for pseudocapacitors.

These POMs properties have been known and studied for several decades. As early as 1997, Gómez-Romero and Lira-Cantú [86] combined POMs with different conducting polymers for SC applications. Over the years, organic-inorganic hybrids comprising polypyrrole (PPy) [87], poly(3,4-ethylenedioxythiophene) (PEDOT), or polyaniline (PANI) [88], and POMs have been reported.

Vanadate POMs and activated carbon were combined as the positive and negative electrodes, respectively, in an asymmetric cell [89]. Such a cell reached a capacitance of 354 F g^{-1}, as well as a specific energy of 73 W h kg^{-1} at 0.1 A g^{-1} and a specific power of 312 W kg^{-1}.

Gupta et al. [90] also delved into the research of POMs for use in supercapacitors, more specifically, into hybrids of phosphomolybdate acid-$H_3PMo_{12}O_{40}$ and phosphotungstic acid-$H_3PW_{12}O_{40}$ with rGO. The effect of this hybridization on the electrochemical properties was very positive and the specific capacitance increased from 70 F g^{-1} measured for rGO to 350 F g^{-1} for the hybrid material. A higher current carrying capacity was also achieved with good retention (94 %), and consequently higher specific energy and specific power density, as shown in Figure 7.

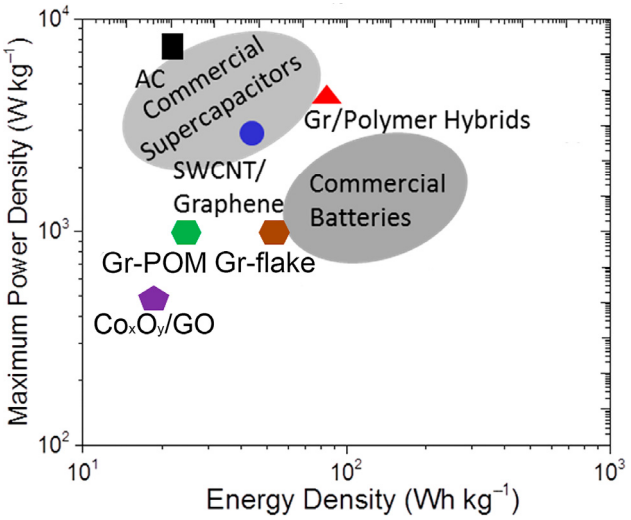

Figure 7. The performance of commercial supercapacitors and batteries, activated carbon, carbon nanotubes/graphene, graphene–polymer hybrids, and graphene–POM electrodes (adapted from [90]).

6. Conclusions

This review recapitulates the main properties of POMs that make them suitable for electrochemical energy conversion and storage applications. Numerous examples of their successful employment in the electrocatalysis of reactions operating water electrolyzers, fuel cells, different types of batteries, and supercapacitors are presented.

POMs exhibit distinctive redox characteristics and the capability of reversibly uptaking as much as 24 electrons per cluster unit. Their redox potential and the number of electrons stored can be tailored additionally by, for instance, the incorporation of redox-active metal centers through a chemical process. One of the main drawbacks of POMs as electrocatalysts is their low electrical conductivity; still, this problem can be overcome by designing composite materials comprising POMs and highly conductive materials such as carbon-based ones.

Consequently, POMs and their composites have been investigated as electrocatalysts for ORR, OER, and HER, sometimes reaching performance comparable to that of commercial Pt/C benchmark electrocatalyst.

POMs and their composites have also been explored as both cathode and anode materials for LIBs and SIBs with LIBs exhibiting especially promising performance. The

lower performance of SIBs employing POMs was considered to be a consequence of the formation of a Na_2O passivating film layer during the first charge/discharge cycles. Still, promising performance can be achieved by tailoring the redox properties and structural design of POMs, resulting in the acceptability of a high number of electrons as well as various pathways of Na^+ ion migration and their easy intercalation. An additional advantage of POMs as electrocatalysts is their recyclability due to their ease of recovery from used electrodes of batteries by simple water treatment. Studies involving RFBs generally showed limited cycling stability and excessive hydrogen production. Nevertheless, several redox-active species have been tested for RFBs throughout the years, with different levels of success.

The potential of POMs as electrode materials for supercapacitors has been recognized early; they indeed demonstrated a high contribution to specific energy and specific power density. However, some challenges regarding POMs as electrode materials for supercapacitors have been encountered, including secure grafting of POMs onto a substrate/host material and attaining a durable cycle life. These challenges are yet to be overcome.

Author Contributions: Conceptualization, B.Š. and D.M.F.S.; investigation, F.M.B.G.; data curation, F.M.B.G., K.R. and D.M.; writing—original draft preparation, F.M.B.G.; writing—review and editing, B.Š. and D.M.F.S.; visualization, F.M.B.G., K.R. and D.M.; supervision, B.Š. and D.M.F.S. All authors have read and agreed to the published version of the manuscript.

Funding: Fundação para a Ciência e a Tecnologia (FCT, Portugal) is acknowledged for funding EXPL/EQU-EQU/0517/2021 project as well as research contract in the scope of programmatic funding UIDP/04540/2020 (D.M.F. Santos) and contract no. IST-ID/156-2018 (B. Šljukić).

Data Availability Statement: Not applicable.

Conflicts of Interest: The authors declare no conflict of interest.

References

1. Santos, D.M.F.; Šljukić, B. Advanced materials for electrochemical energy conversion and storage devices. *Materials* **2021**, *14*, 7711. [CrossRef]
2. Badwal, S.P.S.; Giddey, S.S.; Munnings, C.; Bhatt, A.I.; Hollenkamp, A.F. Emerging electrochemical energy conversion and storage technologies. *Front. Chem.* **2014**, *2*, 79. [CrossRef]
3. Santos, D.M.F.; Šljukić, B.; Sequeira, C.A.C.; Macció, D.; Saccone, A.; Figueiredo, J.L. Electrocatalytic approach for the efficiency increase of electrolytic hydrogen production: Proof-of-concept using platinum-dysprosium alloys. *Energy* **2013**, *50*, 486–492. [CrossRef]
4. Chatenet, M.; Pollet, B.G.; Dekel, D.R.; Dionigi, F.; Deseure, J.; Millet, P.; Braatz, R.D.; Bazant, M.Z.; Eikerling, M.; Staffell, I.; et al. Water electrolysis: From textbook knowledge to the latest scientific strategies and industrial developments. *Chem. Soc. Rev.* **2022**, *51*, 4583–4762. [CrossRef] [PubMed]
5. Chen, J.; Xiao, R.; Fu, K.; Wu, Y.; Guo, Y.; Yang, S.; Li, H.; Zheng, J.; Li, X. Metal hydride mediated water splitting: Electrical energy saving and decoupled H_2/O_2 generation. *Mater. Today* **2021**, *47*, 16–24. [CrossRef]
6. Grigoriev, S.A.; Fateev, V.N.; Bessarabov, D.G.; Millet, P. Current status, research trends, and challenges in water electrolysis science and technology. *Int. J. Hydrog. Energy* **2020**, *45*, 26036–26058. [CrossRef]
7. Wang, H.; Hamanaka, S.; Nishimoto, Y.; Irle, S.; Yokoyama, T.; Yoshikawa, H.; Awaga, K. In operando X-ray absorption fine structure studies of polyoxometalate molecular cluster batteries: Polyoxometalates as electron sponges. *J. Am. Chem. Soc.* **2012**, *134*, 4918–4924. [CrossRef] [PubMed]
8. Kawasaki, N.; Wang, H.; Nakanishi, R.; Hamanaka, S.; Kitaura, R.; Shinohara, H.; Yokoyama, T.; Yoshikawa, H.; Awaga, K. Nanohybridization of polyoxometalate clusters and single-wall carbon nanotubes: Applications in molecular cluster batteries. *Angew. Chemie-Int. Ed.* **2011**, *50*, 3471–3474. [CrossRef]
9. López, X.; Fernández, J.A.; Poblet, J.M. Redox properties of polyoxometalates: New insights on the anion charge effect. *J. Chem. Soc. Dalt. Trans.* **2005**, *6*, 1162–1167. [CrossRef] [PubMed]
10. Wang, H.; Kawasaki, N.; Yokoyama, T.; Yoshikawa, H.; Awaga, K. Molecular cluster batteries of nano-hybrid materials between Keggin POMs and SWNTs. *Dalt. Trans.* **2012**, *41*, 9863–9866. [CrossRef]
11. López, X.; Bo, C.; Poblet, J.M. Electronic properties of polyoxometalates: Electron and proton affinity of mixed-addenda Keggin and Wells-Dawson anions. *J. Am. Chem. Soc.* **2002**, *124*, 12574–12582. [CrossRef] [PubMed]
12. Ji, Y.; Huang, L.; Hu, J.; Streb, C.; Song, Y.F. Polyoxometalate-functionalized nanocarbon materials for energy conversion, energy storage and sensor systems. *Energy Environ. Sci.* **2015**, *8*, 776–789. [CrossRef]

13. Stamate, A.E.; Pavel, O.D.; Zavoianu, R.; Marcu, I.C. Highlights on the catalytic properties of polyoxometalate-intercalated layered double hydroxides: A review. *Catalysts* **2020**, *10*, 57. [CrossRef]
14. Yan, Z.; Liu, H.; Hao, Z.; Yu, M.; Chen, X.; Chen, J. Electrodeposition of (hydro)oxides for an oxygen evolution electrode. *Chem. Sci.* **2020**, *11*, 10614–10625. [CrossRef] [PubMed]
15. Lv, H.; Geletii, Y.V.; Zhao, C.; Vickers, J.W.; Zhu, G.; Luo, Z.; Song, J.; Lian, T.; Musaev, D.G.; Hill, C.L. Polyoxometalate water oxidation catalysts and the production of green fuel. *Chem. Soc. Rev.* **2012**, *41*, 7572–7589. [CrossRef] [PubMed]
16. Geletii, Y.V.; Botar, B.; Kögerler, P.; Hillesheim, D.A.; Musaev, D.G.; Hill, C.L. An all-inorganic, stable, and highly active tetraruthenium homogeneous catalyst for water oxidation. Angew. *Chemie. Int. Ed.* **2008**, *47*, 3896–3899. [CrossRef] [PubMed]
17. Geletii, Y.V.; Huang, Z.; Hou, Y.; Musaev, D.G.; Lian, T.; Hill, C.L. Homogeneous light-driven water oxidation catalyzed by a tetraruthenium complex with all inorganic ligands. *J. Am. Chem. Soc.* **2009**, *131*, 7522–7523. [CrossRef]
18. Besson, C.; Huang, Z.; Geletii, Y.V.; Lense, S.; Hardcastle, K.I.; Musaev, D.G.; Lian, T.; Proust, A.; Hill, C.L. $Cs_9[(\gamma\text{-}PW_{10}O_{36})_2Ru_4O_5(OH)(H_2O)_4]$, a new all-inorganic, soluble catalyst for the efficient visible-light-driven oxidation of water. *Chem. Commun.* **2010**, *46*, 2784–2786. [CrossRef] [PubMed]
19. Toma, F.M.; Sartorel, A.; Iurlo, M.; Carraro, M.; Parisse, P.; MacCato, C.; Rapino, S.; Gonzalez, B.R.; Amenitsch, H.; Da Ros, T.; et al. Efficient water oxidation at carbon nanotube-polyoxometalate electrocatalytic interfaces. *Nat. Chem.* **2010**, *2*, 826–831. [CrossRef] [PubMed]
20. Horn, M.R.; Singh, A.; Alomari, S.; Goberna-Ferrón, S.; Benages-Vilau, R.; Chodankar, N.; Motta, N.; Ostrikov, K.; Macleod, J.; Sonar, P.; et al. Polyoxometalates (POMs): From electroactive clusters to energy materials. *Energy Environ. Sci.* **2021**, *14*, 1652–1700. [CrossRef]
21. Guo, S.X.; Liu, Y.; Lee, C.Y.; Bond, A.M.; Zhang, J.; Geletii, Y.V.; Hill, C.L. Graphene-supported $[\{Ru_4O_4(OH)_2(H_2O)_4\}(\gamma\text{-}SiW_{10}O_{36})_2]^{10-}$ for highly efficient electrocatalytic water oxidation. *Energy Environ. Sci.* **2013**, *6*, 2654–2663. [CrossRef]
22. Quintana, M.; López, A.M.; Rapino, S.; Toma, F.M.; Iurlo, M.; Carraro, M.; Sartorel, A.; MacCato, C.; Ke, X.; Bittencourt, C.; et al. Knitting the catalytic pattern of artificial photosynthesis to a hybrid graphene nanotexture. *ACS Nano* **2013**, *7*, 811–817. [CrossRef]
23. How the Race for Cobalt Risks Turning It from Miracle Metal to Deadly Chemical. Available online: https://www.theguardian.com/global-development/2019/dec/18/how-the-race-for-cobalt-risks-turning-it-from-miracle-metal-to-deadly-chemical (accessed on 20 May 2022).
24. Limani, N.; Marques, I.S.; Jarrais, B.; Fernandes, A.J.S.; Freire, C.; Fernandes, D.M. Cobalt Phosphotungstate-based composites as bifunctional electrocatalysts for oxygen reactions. *Catalysts* **2022**, *12*, 357. [CrossRef]
25. Zaharieva, I.; Chernev, P.; Risch, M.; Klingan, K.; Kohlhoff, M.; Fischer, A.; Dau, H. Electrosynthesis, functional, and structural characterization of a water-oxidizing manganese oxide. *Energy Environ. Sci.* **2012**, *5*, 7081–7089. [CrossRef]
26. Goberna-Ferrón, S.; Soriano-López, J.; Galán-Mascarós, J.R. Activity and stability of the tetramanganese polyanion $[Mn_4(H_2O)_2(PW_9O_{34})_2]^{10-}$ during electrocatalytic water oxidation. *Inorganics* **2015**, *3*, 332–340. [CrossRef]
27. Wu, Y.; Pei, J.; Yu, X.; Bi, L. Study on catalytic water oxidation properties of polynuclear manganese containing polyoxometalates. *Catalysts* **2022**, *12*, 160. [CrossRef]
28. Vij, V.; Sultan, S.; Harzandy, A.; Meena, A.; Tiwari, J.; Lee, W.; Yoon, T.; Kim, K. Nickel–Based Electrocatalysts for Energy Related Applications: Oxygen Reduction, Oxygen Evolution, and Hydrogen Evolution Reactions. *ACS Catalysis.* **2017**, *7*, 7196–7225. [CrossRef]
29. Zhu, G.; Glass, E.N.; Zhao, C.; Lv, H.; Vickers, J.W.; Geletii, Y.V.; Musaev, D.G.; Song, J.; Hill, C.L. A nickel containing polyoxometalate water oxidation catalyst. *Dalt. Trans.* **2012**, *41*, 13043–13049. [CrossRef]
30. Singh, C.; Mukhopadhyay, S.; Das, S.K. Polyoxometalate-supported Bis(2,2′-bipyridine)mono(aqua)nickel(II) coordination complex: An efficient electrocatalyst for water oxidation. *Inorg. Chem.* **2018**, *57*, 6479–6490. [CrossRef]
31. Luo, W.; Hu, J.; Diao, H.; Schwarz, B.; Streb, C.; Song, Y. Robust polyoxometalate/nickel foam composite electrodes for sustained electrochemical oxygen evolution at high pH. *Angew. Chem. Int. Ed.* **2017**, *56*, 4941–4944. [CrossRef]
32. Joshi, A. A rare polyoxometalate cluster $[NiW_{12}O_{44}]_{14}^{-}$ based solid as a pre-catalyst for efficient and long-term oxygen evolution. *Nanoscale Adv.* 2022. [CrossRef]
33. Han, X.; Li, Y.; Zhang, Z.; Tan, H.; Lu, Y.; Wang, E. Polyoxometalate-based nickel clusters as visible light-driven water oxidation catalysts. *J. Am. Chem. Soc.* **2015**, *137*, 5486–5493. [CrossRef]
34. Yu, L.; Lin, J.; Zheng, M.; Chen, M.; Ding, Y. Homogeneous electrocatalytic water oxidation at neutral pH by a robust trinuclear copper(II)-substituted polyoxometalate. *Chem. Commun.* **2018**, *54*, 354–357. [CrossRef] [PubMed]
35. Yu, L.; Du, X.; Ding, Y.; Chen, H.; Zhou, P. Efficient visible light-driven water oxidation catalyzed by an all-inorganic copper-containing polyoxometalate. *Chem. Commun.* **2015**, *51*, 17443–17446. [CrossRef] [PubMed]
36. Azmani, K.; Besora, M.; Soriano-López, J.; Landolsi, M.; Teillout, A.L.; de Oliveira, P.; Mbomekallé, I.M.; Poblet, J.M.; Galán-Mascarós, J.R. Understanding polyoxometalates as water oxidation catalysts through iron vs. cobalt reactivity. *Chem. Sci.* **2021**, *12*, 8755–8766. [CrossRef]
37. Han, X.B.; Tang, X.Y.; Lin, Y.; Gracia-Espino, E.; Liu, S.G.; Liang, H.W.; Hu, G.Z.; Zhao, X.J.; Liao, H.G.; Tan, Y.Z.; et al. Ultrasmall abundant metal-based clusters as oxygen-evolving catalysts. *J. Am. Chem. Soc.* **2019**, *141*, 232–239. [CrossRef] [PubMed]
38. Craig, M.; Barda-Chatain, R.; Garcia-Melchor, M. Fundamental insights and rational design of low-cost polyoxometalates for the oxygen evolution reaction. *J. Catal.* **2021**, *393*, 202–206. [CrossRef]

39. Yin, Q.; Xu, Z.; Lian, T.; Musaev, D.; Hill, C.; Geletii, Y. Tafel Slope Analyses for Homogeneous Catalytic Reactions. *Catalysts* **2021**, *11*, 87. [CrossRef]
40. Zheng, Y.; Xu, X.; Chen, J.; Wang, Q. Surface $O2^{-}$ regulation on POM electrocatalyst to achieve accurate 2e/4e-ORR control for H_2O_2 production and Zn-air battery assemble. *Appl. Catal. B Environ.* **2021**, *285*, 119788. [CrossRef]
41. Marques, I.S.; Jarrais, B.; Mbomekallé, I.M.; Teillout, A.L.; de Oliveira, P.; Freire, C.; Fernandes, D.M. Synergetic Effects of Mixed-Metal Polyoxometalates@ Carbon-Based Composites as Electrocatalysts for the Oxygen Reduction and the Oxygen Evolution Reactions. *Catalysts* **2022**, *12*, 440. [CrossRef]
42. Wang, Y.; Wang, Y.; Zhang, L.; Liu, C.S.; Pang, H. Core–shell-type ZIF-8@ ZIF-67@ POM hybrids as efficient electrocatalysts for the oxygen evolution reaction. *Inorg. Chem. Front.* **2019**, *6*, 2514–2520. [CrossRef]
43. Wang, Y.; Wang, Y.; Zhang, L.; Liu, C.; Pang, H. PBA@ POM hybrids as efficient electrocatalysts for the oxygen evolution reaction. *Chem. Asian J.* **2019**, *14*, 2790–2795. [CrossRef] [PubMed]
44. Singh, C.; Haldar, A.; Basu, O.; Das, S.K. Devising a polyoxometalate-based functional material as an efficient electrocatalyst for the hydrogen evolution reaction. *Inorg. Chem.* **2021**, *60*, 10302–10314. [CrossRef]
45. Cao, J.P.; Fang, T.; Fu, L.Z.; Zhou, L.L.; Zhan, S.Z. First mononuclear copper(II) electro-catalyst for catalyzing hydrogen evolution from acetic acid and water. *Int. J. Hydrog. Energy* **2014**, *39*, 13972–13978. [CrossRef]
46. Xue, D.; Peng, Q.X.; Zhan, S.Z. Synthesis and electrochemical properties of a water soluble nickel(II) complex supported by N-phenylpyridin-2-ylmethanimine ligand. *Inorg. Chem. Commun.* **2017**, *82*, 11–15. [CrossRef]
47. Fang, T.; Fu, L.Z.; Zhou, L.L.; Zhan, S.Z.; Chen, S. Electrochemical-driven water reduction catalyzed by a water soluble cobalt(III) complex with Schiff base ligand. *Electrochim. Acta* **2015**, *178*, 368–373. [CrossRef]
48. Jia, X.; Streb, C.; Song, Y. Devisable POM/Ni Foam Composite: Precisely Control Synthesis toward Enhanced Hydrogen Evolution Reaction at High pH. *Chem. Eur. J.* **2019**, *25*, 15548. [CrossRef] [PubMed]
49. Jana, D.; Kolli, H.; Sabnam, S.; Das, S. Efficient homogeneous electrocatalytic hydrogen evolution using a Ni-containing polyoxometalate catalyst. *Chem. Commun.* **2021**, *57*, 9910–9913. [CrossRef]
50. Wang, X.L.; Tian, Y.; Chang, Z.H.; Lin, H. A Series of polyoxometalate-based metal-bis(pyridyl-tetrazole) complexes with high electrocatalytic activity for hydrogen evolution reaction in alkaline and acid media. *ACS Sustain. Chem. Eng.* **2020**, *8*, 15696–15702. [CrossRef]
51. Fernandes, D.M.; Araújo, M.P.; Haider, A.; Mougharbel, A.S.; Fernandes, A.J.S.; Kortz, U.; Freire, C. Polyoxometalate-graphene electrocatalysts for the hydrogen evolution reaction. *ChemElectroChem* **2018**, *5*, 273–283. [CrossRef]
52. Yang, Y.; Qian, Y.; Li, H.; Zhang, Z.; Mu, Y.; Do, D.; Zhou, B.; Dong, J.; Yan, W.; Qin, Y.; et al. O-coordinated W-Mo dual-atom catalyst for pH-universal electrocatalytic hydrogen evolution. *Sci. Adv.* **2020**, *6*, eaba6586. [CrossRef]
53. Adamson, A.W.; Waltz, W.L.; Zinato, E.; Watts, D.W.; Fleischauer, P.D.; Lindholm, R.D. Photochemistry of transition-metal coordination compounds. *Chem. Rev.* **1968**, *68*, 541–585. [CrossRef]
54. Šljukić, B.; Banks, C.; Compton, R. An overview of the electrochemical reduction of oxygen at carbon-based modified electrodes. *JICS* **2015**, *2*, 1–25. [CrossRef]
55. Zhang, S.; Oms, O.; Hao, L.; Liu, R.; Wang, M.; Zhang, Y.; He, H.Y.; Dolbecq, A.; Marrot, J.; Keita, B.; et al. High oxygen reduction reaction performances of cathode materials combining polyoxometalates, coordination complexes, and carboneous supports. *ACS Appl. Mater. Interfaces* **2017**, *9*, 38486–38498. [CrossRef]
56. Liu, R.; Cao, K.; Clark, A.H.; Lu, P.; Anjass, M.; Biskupek, J.; Kaiser, U.; Zhang, G.; Streb, C. Top-down synthesis of polyoxometalate-like sub-nanometer molybdenum-oxo clusters as high-performance electrocatalysts. *Chem. Sci.* **2020**, *11*, 1043–1051. [CrossRef] [PubMed]
57. Lee, C.; Jeon, D.; Park, J.; Lee, W.; Park, J.; Kang, S.J.; Kim, Y.; Ryu, J. Tetraruthenium polyoxometalate as an atom-efficient bifunctional oxygen evolution reaction/oxygen reduction reaction catalyst and its application in seawater batteries. *ACS Appl. Mater. Interfaces* **2020**, *12*, 32689–32697. [CrossRef] [PubMed]
58. Sanij, F.; Balakrishnan, P.; Su, H.; Khotseng, L.; Xu, Q. Fabrication of polyoxometalate-modified palladium–nickel/reduced graphene oxide alloy catalysts for enhanced oxygen reduction reaction activity. *RSC Adv.* **2021**, *11*, 39118–39129. [CrossRef]
59. Fernandes, D.; Novais, H.; Bacsa, R.; Serp, P.; Bachiller-Baeza, B.; Rodríguez-Ramos, I.; Guerrero-Ruiz, A.; Freire, C. Polyoxotungstate@ carbon nanocomposites as oxygen reduction reaction (ORR) electrocatalysts. *Langmuir* **2018**, *34*, 6376–6387. [CrossRef] [PubMed]
60. Ni, E.; Uematsu, S.; Tsukada, T.; Sonoyama, N. Lithium intercalation into polyoxomolybdate $(NH_4)_6[NiMo_9O_{32}]$ as the cathode material of lithium battery. *Solid State Ion.* **2016**, *285*, 83–90. [CrossRef]
61. Ji, Y.; Hu, J.; Huang, L.; Chen, W.; Streb, C.; Song, Y.F. Covalent attachment of Anderson-type polyoxometalates to single-walled carbon nanotubes gives enhanced performance electrodes for lithium ion batteries. *Chem. A Eur. J.* **2015**, *21*, 6469–6474. [CrossRef] [PubMed]
62. Pan, F.; Wang, Q. Redox species of redox flow batteries: A review. *Molecules* **2015**, *20*, 20499–20517. [CrossRef] [PubMed]
63. Lyu, Y.; Liu, Y.; Yu, Z.E.; Su, N.; Liu, Y.; Li, W.; Li, Q.; Guo, B.; Liu, B. Recent advances in high energy-density cathode materials for sodium-ion batteries. *Sustain. Mater. Technol.* **2019**, *21*, e00098. [CrossRef]
64. Liu, J.; Chen, Z.; Chen, S.; Zhang, B.; Wang, J.; Wang, H.; Tian, B.; Chen, M.; Fan, X.; Huang, Y.; et al. "Electron/Ion Sponge"-like V-based polyoxometalate: Toward high-performance cathode for rechargeable sodium ion batteries. *ACS Nano* **2017**, *11*, 6911–6920. [CrossRef] [PubMed]

65. Chen, J.J.; Ye, J.C.; Zhang, X.G.; Symes, M.D.; Fan, S.C.; Long, D.L.; Zheng, M.S.; Wu, D.Y.; Cronin, L.; Dong, Q.F. Design and performance of rechargeable sodium ion batteries, and symmetrical Li-Ion batteries with supercapacitor-like power density based upon polyoxovanadates. *Adv. Energy Mater.* **2018**, *8*, 1701021. [CrossRef]
66. Hartung, S.; Bucher, N.; Chen, H.Y.; Al-Oweini, R.; Sreejith, S.; Borah, P.; Yanli, Z.; Kortz, U.; Stimming, U.; Hoster, H.E.; et al. Vanadium-based polyoxometalate as new material for sodium-ion battery anodes. *J. Power Sources* **2015**, *288*, 270–277. [CrossRef]
67. Lin, C.C.; Lin, W.H.; Huang, S.C.; Hu, C.W.; Chen, T.Y.; Hsu, C.T.; Yang, H.; Haider, A.; Lin, Z.; Kortz, U.; et al. Mechanism of sodium ion storage in $Na_7[H_2PV_{14}O_{42}]$ anode for sodium-ion batteries. *Adv. Mater. Interfaces* **2018**, *5*, 1800491. [CrossRef]
68. Yuan, X.Z.; Song, C.; Platt, A.; Zhao, N.; Wang, H.; Li, H.; Fatih, K.; Jang, D. A review of all-vanadium redox flow battery durability: Degradation mechanisms and mitigation strategies. *Int. J. Energy Res.* **2019**, *43*, 6599–6638. [CrossRef]
69. Xia, S.; Li, F.; Li, X.; Cheng, F.; Sun, C.; Liu, J.-J.; Guo, H. An inorganic–organic hybrid supramolecular framework as a high-performance anode for lithium-ion batteries. *Dalton Trans.* **2018**, *47*, 5166. [CrossRef]
70. Zhang, A.; Zhang, M.; Lan, D.; Lan, D.; Wang, H.; Tang, Y.; Wang, X.; Dong, L.; Zhang, L.; Li, S.; et al. Polyoxometalate-Based Metal-Organic Framework on Carbon Cloth with a Hot-Pressing Method for High-Performance Lithium-Ion Batteries. *Inorg Chem.* **2018**, *57*, 11726–11731. [CrossRef]
71. Wei, T.; Zhang, M.; Wu, P.; Tang, Y.-J.; Li, S.-L.; Shen, F.-C.; Wang, X.-L.; Zhou, X.-P.; Lan, Y.-Q. POM-based metal-organic framework/reduced graphene oxide nanocomposites with hybrid behavior of battery-supercapacitor for superior lithium storage. *Nano Energy* **2017**, *34*, 205. [CrossRef]
72. Hu, J.; Jia, F.; Song, Y.-F. Engineering high-performance polyoxometalate/PANI/MWNTs nanocomposite anode materials for lithium ion batteries. *Chem. Eng. J.* **2017**, *326*, 273. [CrossRef]
73. Iqbal, B.; Jia, X.; Hu, H.; He, L.; Chen, W.; Song, Y. Inorg. *Chem. Front.* **2020**, *7*, 1420–1427. [CrossRef]
74. Chen, J.; Symes, M.; Fan, S.; Zheng, M.; Miras, H.; Dong, Q.; Cronin, L. High-Performance Polyoxometalate-Based Cathode Materials for Rechargeable Lithium-Ion Batteries. *Adv. Mater.* **2015**, *27*, 4649–4654. [CrossRef] [PubMed]
75. Cao, D.; Sha, Q.; Wang, J.; Li, J.; Ren, J.; Shen, T.; Bai, S.; He, L.; Song, Y. Advanced Anode Materials for Sodium-Ion Batteries: Confining Polyoxometalates in Flexible Metal-Organic Frameworks by the "Breathing Effect". *ACS Appl. Mater. Interfaces* **2022**, *14*, 22186–22196. [CrossRef] [PubMed]
76. Yang, L.; Hao, Y.; Lin, J.; Li, K.; Luo, S.; Lei, J.; Han, Y.; Yuan, R.; Liu, G.; Ren, B.; et al. POM Anolyte for All-Anion Redox Flow Batteries with High Capacity Retention and Coulombic Efficiency at Mild pH. *Adv. Mater.* **2022**, *34*, 2107425. [CrossRef] [PubMed]
77. Dubal, D.P.; Rueda-Garcia, D.; Marchante, C.; Benages, R.; Gomez-Romero, P. Hybrid graphene-polyoxometalates nanofluids as liquid electrodes for dual energy storage in novel flow cells. *Chem. Rec.* **2018**, *18*, 1076–1084. [CrossRef] [PubMed]
78. Horn, M.; MacLeod, J.; Liu, M.; Webb, J.; Motta, N. Supercapacitors: A new source of power for electric cars? *Econ. Anal. Policy* **2019**, *61*, 93–103. [CrossRef]
79. Clemente, A.; Costa-Castelló, R. Redox flow batteries: A literature review oriented to automatic control. *Energies* **2020**, *13*, 4514. [CrossRef]
80. Ulaganathan, M.; Aravindan, V.; Yan, Q.; Madhavi, S.; Skyllas-Kazacos, M.; Lim, T.M. Recent Advancements in all-vanadium redox flow batteries. *Adv. Mater. Interfaces* **2016**, *3*, 1500309. [CrossRef]
81. Wei, X.; Pan, W.; Duan, W.; Hollas, A.; Yang, Z.; Li, B.; Nie, Z.; Liu, J.; Reed, D.; Wang, W.; et al. Materials and systems for organic redox flow batteries: Status and challenges. *ACS Energy Lett.* **2017**, *2*, 2187–2204. [CrossRef]
82. Pratt, H.D.; Anderson, T.M. Mixed addenda polyoxometalate "solutions" for stationary energy storage. *Dalt. Trans.* **2013**, *42*, 15650–15655. [CrossRef] [PubMed]
83. Zhao, Y.; Liu, J.; Wang, N.; Li, Q.; Hu, M. Rational selection of small aromatic molecules to functionalize graphene for enhancing capacitive energy storage. *J. Mater. Chem. A* **2018**, *6*, 7566–7572. [CrossRef]
84. Han, Y.; Lan, J.; Li, K.; Yang, L.; Zhu, C.; Chen, J. The Cluster Design and Redox Behavior Characterization of Polyoxometalates for Redox Flow Batteries. *Chem. Asian J.* **2022**, e202200950. [CrossRef]
85. Horn, M.; Gupta, B.; MacLeod, J.; Liu, J.; Motta, N. Graphene-based supercapacitor electrodes: Addressing challenges in mechanisms and materials. *Curr. Opin. Green Sustain. Chem.* **2019**, *17*, 42–48. [CrossRef]
86. Gómez-Romero, P.; Lira-Cantú, M. Hybrid organic-inorganic electrodes: The molecular material formed between polypyrrole and the phosphomolybdate anion. *Adv. Mater.* **1997**, *9*, 144–147. [CrossRef]
87. Gómez-Romero, P.; Chojak, M.; Cuentas-Gallegos, K.; Asensio, J.A.; Kulesza, P.J.; Casañ-Pastor, N.; Lira-Cantú, M. Hybrid organic-inorganic nanocomposite materials for application in solid state electrochemical supercapacitors. *Electrochem. Commun.* **2003**, *5*, 149–153. [CrossRef]
88. Cuentas-Gallegos, A.K.; Lira-Cantú, M.; Casañ-Pastor, N.; Gómez-Romero, P. Nanocomposite hybrid molecular materials for application in solid-state electrochemical supercapacitors. *Adv. Funct. Mater.* **2005**, *15*, 1125–1133. [CrossRef]
89. Chen, H.Y.; Wee, G.; Al-Oweini, R.; Friedl, J.; Tan, K.S.; Wang, Y.; Wong, C.L.; Kortz, U.; Stimming, U.; Srinivasan, M. A polyoxovanadate as an advanced electrode material for supercapacitors. *ChemPhysChem* **2014**, *15*, 2162–2169. [CrossRef] [PubMed]
90. Gupta, S.; Aberg, B.; Carrizosa, S. Functionalized graphene–polyoxometalate nanodots assembly as "organic–inorganic" hybrid supercapacitors and insights into electrode/electrolyte interfacial processes. *C—J. Carbon Res.* **2017**, *3*, 24. [CrossRef]